Electrochemical noise measurements on stainless steel using a gelled electrolyte

Gleidys Monrrabal, François Huet, Asunción Bautista

Electrochemical noise measurements on stainless steel using a gelled electrolyte

Gleidys Monrrabal[a,b], François Huet[b,*], Asunción Bautista[a]

[a] *Materials Science and Engineering Department, IAAB, Universidad Carlos III de Madrid, Avda. Universidad n° 30, 28911 Leganés, Madrid, Spain*

[b] *Sorbonne Université, CNRS, Laboratoire Interfaces et Systèmes Electrochimiques, LISE, F-75005 Paris, France*

ABSTRACT

The present paper presents pioneering results about the use of the electrochemical noise (EN) technique to study corrosion of metal surfaces of complex geometry in a gel electrolyte based on agar-glycerol, the composition of which was previously optimized for electrochemical measurements on stainless steel (SS) surfaces. EN results obtained with AISI 304 SS electrodes in both gelled and liquid electrolytes using three different modes (zero-resistance ammeter, potentiostatic, galvanostatic) of measurements have been compared and discussed. Tests carried out in gel allow the possibilities and limitations of using portable gel cells for monitoring corrosion of SS complex surfaces to be determined.

Keywords: electrochemical noise, gelled electrolyte, stainless steel, pitting corrosion, potentiostatic, galvanostatic

[*] Corresponding author.

E-mail address: francois.huet@sorbonne-universite.fr (F. Huet)

1. Introduction

Electrochemical noise (EN) is a powerful technique providing information about corrosion processes, such as mechanism and rate. Indeed, the measurement of spontaneous current and/or potential fluctuations gives access in real time to corrosion events, which cannot be obtained by conventional deterministic electrochemical methods such as the linear polarization resistance technique, cyclic voltammetry, and electrochemical impedance spectroscopy (EIS) that provide information averaged in time and on the electrode surface area.

EN has received considerable attention in the corrosion domain since the pioneering works of Hagyard and Prior [1] and Iverson [2]. EN has been developed for studying all types of corrosion, from uniform corrosion to localized corrosion, such as pitting corrosion, crevice corrosion, or stress corrosion cracking, especially in the passivity domain for investigating the breakdown and repair of passive films [3-8]. Before the 1990s, EN was measured under potentiostatic or galvanostatic control using a single corroding electrode. In the first case, the potential of the tested electrode is fixed versus a reference electrode (RE) and the fluctuations of the current flowing through the working electrode (WE) are recorded. In the galvanostatic mode, the current is fixed and the fluctuations of the electrode potential are recorded against the RE. However, both methods are limited by the fact that the corrosion rate of the WE cannot be obtained from measuring either current fluctuations or potential fluctuations. With the aim of overcoming this limitation, a new cell configuration was proposed in 1986 consisting in coupling two freely corroding identical WEs connected through a zero-resistance ammeter (ZRA) and using a RE [9]. Both potential and current fluctuations can then be measured, from which is derived the noise resistance (R_n), defined as the ratio of the standard deviations of the potential and current fluctuations. R_n is related to the corrosion rate via Stern and Geary relationship [4,9-11]. It is important to note that a zero potential difference is maintained between the WEs by the ZRA; as a consequence, both WEs are at their open-circuit potential (OCP) and the *d.c.* current flowing between them remains close to zero.

Although EN has frequently been used for corrosion monitoring in liquid solutions, it has not yet been used in gel electrolytes. Different gel-phase electrolytes have been proposed for diverse innovative applications during the last years to avoid the handling difficulties encountered with liquid electrolytes [12]. The manufacturing of electrochemical cells with gel electrolytes has already shown some advantages, as the ability to cover different angled surfaces and its easiness to be used as portable electrochemical cell for in-situ corrosion monitoring [13-15]. The formulation of the gel electrolyte used in the present work has been optimized in a previous study [16]. It comprises glycerol, which acts as plasticizer and is responsible for the adaptability of the cell, and agar, which provides the mechanical stability of the electrolyte required for the measurements on portable devices and contributes to the conductivity of the gel. The desired corrosivity of the gel electrolyte is achieved through NaCl addition, which also helps to provide an adequate conductivity to the electrolyte.

The usefulness of this innovative electrolyte has already been tested for studying corrosion of stainless steel (SS) surfaces with complex geometry using *d.c.* polarization techniques [16] and EIS measurements [17]. The present paper presents a pioneering study on the use of the EN technique in ZRA, galvanostatic, and potentiostatic modes for investigating electrochemical processes in an electrochemical cell with gel electrolyte. The EN results were compared to those obtained in a conventional liquid electrolyte with the same NaCl content. Moreover, a portable cell with gel electrolyte was tested with the aim of validating its use to study corrosion processes using EN measurements.

2. Experimental

The (w/w) composition of the gel electrolyte used to carry out the electrochemical studies was 40% glycerol (purity 99%, 1.26 g/cm^3), 0.5% NaCl (purity 99%) and 0.5% agar (strength gel 1.5% (Nikan method), 700-1100 g/cm^3). The double helices of the gel structure form a weakly cross-linked three dimensional polymer network with interstitial spaces filled with the aqueous NaCl solution and glycerol. The reagents were dissolved in distilled water and heated to 90°C under magnetic stirring.

The mixture was stirred continuously for 10 min and then cured in a controlled environment where the temperature and relative humidity were kept at 20°C and 80%, respectively. More information about the gel manufacturing process can be found in a previous publication [16]. The conductivity of the gel electrolyte at room temperature was 3.5 mS cm^{-1}, its pH 6.6, its oxygen content 2.9 ppm, and its viscosity around 2 Pa s [16,17]. A liquid electrolyte consisting of a 0.5 wt % liquid solution of NaCl was used to compare the EN signals generated by the corrosion processes.

Three experimental setups were employed to carry out the electrochemical measurements (Fig. 1), the first one with 2 identical WEs connected with a ZRA, the second one with a single WE and a counter-electrode (CE) used in potentiostatic and galvanostatic modes, and the third one being the portable-gel cell used in potentiostatic and galvanostatic modes. In the following, the two first cells (Figs. 1a and 1b) will be called lab-liquid cell or lab-gel cell, depending on the nature of the electrolyte. A saturated calomel electrode (SCE) was used as RE in all cells. In potentiostatic and galvanostatic modes, the CE was a platinum mesh. AISI 304 SS square-shaped electrodes, the chemical composition of which is shown in Table 1, were used as WE. They were prepared from as-received cold-rolled, unsensitized, and annealed steel sheets. The electrical contact was ensured by a conductive wire that was glued to the back surface of the WE. After polishing with a SiC paper up to 600 grit, and cleaning with alcohol in an ultrasound bath, the side and back surfaces of the WE were insulated with an epoxy coating so that the metal exposed to the electrolyte was a square of surface area 2 cm^2. In ZRA mode (Fig. 1a), the two identical SS WEs were separated by a distance of about 1 cm, and the SCE was placed between them. In the same way, in potentiostatic and galvanostatic modes, the distance between the single WE and the platinum CE was about 1 cm and the RE was placed in the middle (Fig. 1b). Obviously, for the experiments with the gel electrolyte, the three electrodes were immersed in the electrochemical cell when the electrolyte was not yet gelled. All experiments were performed at room temperature in stagnant electrolyte.

A portable cell (Fig. 1c) was also employed in galvanostatic and potentiostatic mode measurements. The cell was a methacrylate cylinder of inner diameter 1.6 cm so that the surface area

of the gel electrolyte in contact with the AISI 304 SS WE (square specimens of side 2.5 cm) was also 2 cm^2. A 316 SS coiled wire of approximately 10 cm^2 in surface area was used as CE and the tip of a Lugging capillary connected to the RE was located close to the WE-gel interface. The distances between the CE and WE and between the WE and the tip of the Lugging capillary were 0.6 cm and 0.3 cm, respectively.

A Gamry Reference 600 galvanostat/potentiostat was used to perform the electrochemical measurements carried out in the three cells as follows. After monitoring the OCP for 1 h, EIS measurements were performed in potentiostatic mode at this potential in the frequency range [10 mHz, 10 kHz] by applying a 10 mV_{rms} sinusoidal perturbation. Then, about 1h 30 min after electrode immersion, the electrode was polarized in galvanostatic or potentiostatic mode (no polarization was applied in ZRA mode) and EN data were acquired sequentially at different sampling frequencies (f_s = 100 Hz during 5 min, f_s = 10 Hz during 9 min, and then f_s = 1 Hz during 2 h) with the ESA 410 software of the Reference 600 instrument. With the aim of controlling the stability of the system and detecting possible changes in the corrosion mechanism, new EN measurements at f_s = 100 Hz and 10 Hz were usually carried out after the long-duration recording at f_s = 1Hz. The power spectral densities (PSDs) of the acquired signals were calculated with the program *psd-detrend_ECG-COMON.exe* based on the fast Fourier transform (Welch periodogram) and a linear detrending of the raw data [18]. It can be downloaded for free from the website of the European Cooperative Group on Corrosion Monitoring of Nuclear Materials (www.ecg-comon.org).

Potentiodynamic polarization curves were previously measured at a sweeping rate of 1.2 mV/s before performing the EN measurements with new samples to determine the pitting potential of the AISI 304 SS in the liquid and gel electrolytes, and select the potential and current at which the WE will be polarized during the EN measurements in potentiostatic and galvanostatic modes. The morphology of the corrosion attack on the SS samples after the EN measurements in potentiostatic and galvanostatic modes was studied by optical microscopy (Motic BA310MET-H with Moticam 1080 camera). In some experiments with the lab-liquid and lab-gel cells, crevice corrosion was

observed on the WE at the boundaries of the surface coated with epoxy resin. In that case, the EN data were discarded in the paper.

3. Results and discussion

3.1. EN measurements in ZRA mode

Fig. 2 shows the voltage and current time records acquired at a sampling rate of 1 Hz in ZRA mode at the OCP in the lab-liquid and lab-gel cells. In both electrolytes, typical values of the mean potential of SS in passive state in 0.5% NaCl solution were obtained with current mean values in the nA range indicating that both WEs had the same OCP value. Both potentials were drifting, with more marked variations in liquid electrolyte than in gel, as also previously observed [16], which suggests slower changes of the chemical composition of the passive layer in gel due to mass transport limitation and lower oxygen content.

Fig. 2 also shows current transients of low amplitude (a few nA), indicating the occurrence of small metastable pits on the surface of the SS in gel and liquid electrolytes. The current transients were in both directions depending on which electrode pitting occurred while all potential transients were in the cathodic direction, as usual for pitting corrosion. Current transients are shown in Fig. 2 to be much less numerous in the gel electrolyte, with a smaller amplitude and a slower repassivation time than in the liquid solution. This could easily be explained by mass transport limitation in the gel electrolyte, which delays the arrival of chloride ions and hinders the removal of corrosion products. The conductivity of the gel electrolyte, which is three times lower than that of the liquid electrolyte [16], may also limit the formation of corrosion cells on the SS surface.

To strengthen the analysis of the electrochemical signals, the PSDs of all time records were calculated using the periodogram method based on the fast Fourier transform. In Fig. 3, the good overlap of the PSDs of the voltage and current noises measured in the lab-liquid and lab-gel cells at different sampling frequencies validates the EN measurements [19]. In this figure, the PSD decreases at frequencies slightly lower than half of the sampling frequencies have been plotted to prove the

existence of anti-aliasing filters in the potentiostat used, which are at the origin of the good overlap of the PSDs, in contrast to most commercial potentiostats [18].

Fig. 3a shows that the voltage PSDs in both electrolytes are identical at frequencies above 1 Hz, indicating that the noise at these frequencies was generated by the potentiostat. Considering that the PSD of the voltage noise due to the instrumentation is about 10^{-10} V^2 Hz^{-1} at 10 mHz [18], it can be stated that the low-frequency part of the voltage noise measured in the lab-gel cell was only slightly higher than the instrumentation noise. In the lab-liquid cell, the amplitude of the voltage noise was larger but it is difficult to relate the PSD shape to the tiny voltage transients that can be seen in Fig. 2a because of the large, slow voltage variations. In contrast, the current noise was mainly due to corrosion processes in both electrolytes, with the possible exception of frequencies higher than 1 Hz in the lab-gel cell where the noise was probably due to the instrumentation. Apart from the PSD increase at very low frequencies for the lab-liquid cell, which is due to slow, large current variations also observed for the voltage signal, both PSDs show a plateau around 50 mHz followed by a decrease in $f^{-\alpha}$, with α values close to 2 for the lab-gel cell and 0.7 for the lab-liquid cell. These values are related to the shape of the current transients. In the lab-gel cell all current transients show a sudden change and an exponential recovery, while triangle and hump shaped transients were also observed in the lab-liquid cell. The values of the cut-off frequency, f_c, of the current PSDs, defined as the intercept between the lines defining the low-frequency plateau and the PSD decrease in a log-log scale, are 45 mHz and 110 mHz for the lab-gel and lab-liquid cell, respectively. This confirms that the repassivation time constant of the pits, which is inversely proportional to f_c, is faster in the lab-liquid cell, as already observed in Fig. 2.

Another way to validate noise measurements in ZRA mode using two identical electrodes consists in comparing the noise impedance, Z_n, defined as the square root of the ratio of the PSDs of the voltage and current fluctuations, to the modulus of the impedance, $|Z|$, of the electrodes. Indeed, it has been shown that when using a true reference electrode, Z_n is equal to $|Z|$ as long as the noise due to the instrumentation is not predominant [20].The Bode diagram in Fig. 4 shows that, for a given

electrolyte, both electrodes had the same impedance, the impedance modulus being slightly higher for the liquid electrolyte, except at high frequencies because of the lower conductivity of the gel electrolyte. As expected, the values of the noise impedance correspond to $|Z|$ in the frequency range in which the noise generated by the corrosion processes is larger than the instrumentation noise (f < 0.5 Hz in the lab-liquid cell and f < 0.1 Hz in the lab-gel cell).

These preliminary results show the possibility of carrying out EN measurements in gel electrolytes. Consistently with the amplitude in the nA range of the current transients generated by metastable pitting, the pits on the surface of the SS electrodes were very small and undetectable by optical microscopy, confirming the passivity of the studied metal at the OCP in gel and liquid electrolytes. The results also give a first insight into the change in pitting behaviour due to mass transport limitation in gelled electrolytes.

However, the ZRA mode cannot be used in practical applications with the portable cell shown in Fig. 1 that comprises a single working electrode. As the usability of the portable cell offers clear advantages for certain applications, in particular for monitoring corrosion of non-flat metal surfaces or reducing the risk of crevice corrosion, EN measurements in potentiostatic and galvanostatic modes were also performed in this study. These modes, which do not entail the use of two identical WEs, allow investigations at anodic potentials, that is, in more aggressive conditions than at the OCP in ZRA mode.

Polarization curves were measured to determine the potentials (resp. currents) at which potentiostatic (resp. galvanostatic) EN measurements should be carried out. As shown in Fig. 5, the OCP of the SS electrodes was roughly 50 mV more anodic in the liquid solution than in the gelled electrolyte while the pitting potential (E_{pit}) was more anodic, so the length of the passive region was similar for the three cells. No meaningful differences were found in the polarization behaviour of the SS in the lab-gel cell and portable cells. The dissolution rate of the metal in the passive domain was slowed down by diffusion limitation of the metal cations in gel, leading to lower current values than

in the liquid electrolyte, and to the linear (in semi-log scale) increase of the anodic current response with increasing potentials measured at a relatively high sweeping rate (1.2 mV/s).

3.2. EN measurements in potentiostatic mode

Tests were carried out at anodic potentials ranging between 150 and 350 mV *vs.* SCE with the aim of selecting conditions where pitting corrosion occurs. Table 2 shows that at potentials below E_{pit} stable pits were formed in the gel electrolyte while only metastable pits could be observed in the liquid electrolyte. This can probably be explained by a higher concentration of metal cations at the dissolving pit surface in the gel electrolyte because of diffusion limitation outside the pit, which enhanced the concentration of chlorides for charge neutrality and produced a more aggressive anolyte inside the pit that was able to sustain the stability of the pit [21]. In addition, in potentiostatic mode undesired crevice corrosion at the edge of the epoxy resin was present in the lab-liquid and lab-gel cells, especially as the anodic overpotential increased. This phenomenon is usually triggered by the formation of a differential aeration cell, due to the depletion of oxygen in the stagnant electrolyte trapped below the epoxy resin when delaminated, which forms an anodic area leading to the onset of crevice corrosion at the metal surface, while cathodic oxygen reduction occurs on the central part of the WE (Fig. 6a) [22]. In contrast, the use of gel electrolyte in the portable cell eliminates the risk of crevice corrosion initiation in electrochemical measurements. Indeed, the external part of the WE in contact with the gel is oxygen-richer than the remaining surface of the electrode (Fig. 6b). Hence, this boundary region would act as a cathode and crevice corrosion should be prevented. This strategy of making cathodic the border of the WE to avoid crevice corrosion in pitting studies is close to that of the Avesta cell [23], but it requires no dilution of the electrolytic medium during the test. Moreover, the implementation of the portable cell for measurements on non-flat substrates is feasible and easy.

From all the experiments carried out potentiostatically, data obtained at 200 mV *vs.* SCE have been chosen to focus briefly on the most relevant results. Fig. 7a shows a current time record measured in the lab-liquid cell and Fig. 7b presents the PSDs corresponding to the current time

records sampled sequentially at 100 Hz (curve *i*), 10 Hz (curve *ii*), 1 Hz (curve *iii*), and 100 Hz (curve *iv*). In liquid NaCl electrolyte, in the absence of crevice corrosion, very frequent current transients of amplitude in the µA range took place during the onset of the anodic polarization (Fig. 7a). Then, the number and amplitude of the current transients progressively decreased until repassivation was complete. After about 2 h of exposure at 200 mV *vs*. SCE, the passivity current reached a stationary value of 0.15 µA and very few transients could then be observed, which explains the very low level of the PSD (curve *iv*). In comparison with the experiments at the OCP in ZRA mode (Fig. 2a), the current transients were more numerous and of higher amplitude at the anodic potential. Furthermore, it can be noticed that they had different shapes. Even if the nucleation and growth of the pits can be considered quite similar at both potentials, the transients reveal a difference in the repassivation time constant. While in ZRA mode the repassivation process of the small pits was slow since it was controlled by the cathodic reactions at the OCP, the repassivation of the much larger pits in potentiostatic mode was much faster due to a sudden commutation from active to passive state of dissolution, as often observed for iron and iron-base alloys [3]. The PSDs in Fig. 7b do not show a good overlap in common frequency ranges, contrary to Fig. 3. This is due to the pit generation process that was not stationary in time, so the relevance of PSDs calculated on long time records, such as for curve *iii*, is questionable. However, it is clear that the decrease in amplitude of the PSDs at low frequency with time comes from the scarcity of the pitting transients. Ten minutes later (curve *iv*), the transients were so rare that the current fluctuations were in fact due to the noise of the potentiostat, as shown by the increase of the PSD with frequency. Indeed, in potentiostatic mode, the PSD of the current noise generated by the instrumentation is equal to the ratio $\Psi_{V_{\mathrm{reg}}} \big/ |Z|^2$, where $\Psi_{V_{\mathrm{reg}}}$ is the PSD of the voltage control noise measured between the RE and the WE, and $|Z|$ is the impedance modulus of the WE [24]. Since $|Z|$ decreases in f^{-2} as the frequency increases between 1 Hz and 50 Hz, while $\Psi_{V_{\mathrm{reg}}}$ varies within less than one decade (see Fig. 3a), the PSD of the current noise of the potentiostat increases with frequency. By the way, both curves *i* and *iv* have the same amplitude at

40 Hz, which indicates that the high frequency part of curve *i* was also originating from the potentiostat noise.

Curiously, no current PSD increasing with frequency was measured in ZRA mode (Fig. 3b) while the amplitude of the current fluctuations was in the same range (nA) as in potentiostatic mode after 2 h of immersion in solution. This can be explained by a higher current-measuring resistor, R_m = 2 MΩ (I/E range = 60 nA) used in ZRA mode than in potentiostatic mode, R_m = 20 kΩ (I/E range = 6 µA). In the latter case, the amplitude of the potential difference across R_m was too low (about 20 μV_{pp}) so that the signal was corrupted by the voltage noise of the differential amplifier across R_m. More precisely, it can be shown that, unlike in the potentiostatic mode, the expression of the PSD of the current noise due to the ZRA contains a term proportional to R_m^{-2}, which has all the more influence on the current measured that R_m is small [25].

In gel electrolyte, the behaviour of the current fluctuations was quite different (Fig. 8). When the SS WE was polarized at 200 mV *vs.* SCE in the lab-gel cell, the current remained at a low value (0.5 µA) during a few hundreds of seconds with very rare pitting transients (Fig. 8a) until a stable pit started growing. The current increased almost linearly and reached a value of 2.7 mA after the 2-h EN measurement at f_s = 1 Hz. So, initially, the passive layer seemed less prone to pitting corrosion in the gel electrolyte than in the liquid solution (Fig. 7a), as already observed in ZRA mode at the OCP according to the lower level of the current PSD at high frequency in the lab-gel cell (Fig. 3b) indicating rarer and weaker metastable pitting transients. However, after a few minutes in the gel electrolyte an initiated pit could not repassivate and became stable. With the portable-gel cell, the same phenomenon took place (Fig. 8b). Very rare transients of amplitude 20 nA (against 1 µA in the lab-gel cell) could be observed during the five first minutes of immersion, and, after about one hour of immersion, the current increased abruptly to reach a value of 7.3 mA after the 2-h EN measurement at f_s = 1 Hz . The slope of the current increase changed with time, probably due to the initiation and growth of several stable pits. It must be noticed that significant local acidification of the solution inside the pits occurred when the SS was polarized in gel, as bubbles could be seen in the electrolyte

after the measurements, presumably hydrogen bubbles generated cathodically in addition to oxygen reduction. The local acidification is related to the intensity of the corrosion attack inside the pits and to lower ion mobility, which favours the continuous dissolution of the metal in the stable pits.

Optical microscopic observations of all SS samples polarized potentiostatically at 200 mV *vs.* SCE confirm that they suffered pitting attack. The metastable pits generated on the SS in liquid electrolyte during the polarization were small and irregular (Fig. 9a) while the stable pits grown in gel were much bigger with rounded shapes (Fig. 9b**).**

It can be concluded that, in liquid electrolyte, the potentiostatic method tends to favour crevice corrosion and metastable pitting at moderate overpotentials, while in gel electrolyte the method is too aggressive for investigating metastable pitting of SS since the current may dramatically increase and lead to the formation of stable pits. Hence, it is worth trying another method, as the galvanostatic testing, to avoid the current drift and the initiation of stable pits in gel electrolytes during the EN measurements.

3.3. EN measurements in galvanostatic mode

In galvanostatic mode, an anodic current of 2.5 µA (current density of 1.25 µA/cm^2) was applied in liquid as well as in gel media. This current density was chosen to polarize the SS WE in the passivity domain in both media with the aim of checking the ability of the EN technique to monitor the nucleation and growth of metastable pits without the formation of stable pits, as observed in the gel electrolyte in potentiostatic mode.

Fig. 10 shows the time records successively acquired at 100 Hz, 10 Hz and 1 Hz in the three cells. Time 0 corresponds to the immersion of the electrodes in solution. As soon as the current of 2.5 µA was applied, the electrode potential drifted towards the pitting potential. Some transients of high peak-to-peak amplitude (up to 40 mV in the lab-gel cell) associated to the initiation of metastable pits can already be observed in the time records sampled at 100 Hz (curves *i*) for both lab-liquid and lab-gel cells. Then, the amplitude of the voltage fluctuations increased and became very large (from 0.6

V to 0.1 V in the lab-liquid cell, from 0.4 V to 0.15 V in the lab-gel cell, and from 0.35 V to 0.15 V in the portable cell). This phenomenon, which occurred much faster in the portable cell, did not correspond to pitting corrosion but to oscillations between the pitting potential of the SS in the considered medium and lower potentials in the passive domain (see Fig. 5). This can be explained from the galvanostatic control of the SS electrode in the passivity domain: when corrosion occurs, the electrode potential is shifted in less noble direction and the system switches between two different states. After some time (for these experiments, 10 min for the portable cell after applying the anodic current against 33 min for the lab-gel cell), the oscillations stopped and the electrode potential drifted to values close to the OCP, indicating that the electrode became passive again.

Even if the current fluctuations were not stationary, as shown in Fig. 10, the PSDs were calculated for the different time records successively sampled in the order *i* to *v*. For the time records showing the transition from high to low potentials (curve *iii* in the lab-liquid cell, curve *ii* for the portable cell), the records were split in two parts, before and after the transition, and the PSDs were calculated in both parts. In the lab-liquid cell, the intensity of the potential noise due to metastable pitting increased with time, which explains the non-overlap of curves *i*, *ii* and *iii* in Fig. 11a, till the transition to passivation. After the transition, the PSD decreased drastically to reach a level (curves *iv* and *v*) below that of the voltage noise of the instrumentation in galvanostatic mode, which is slightly higher than in ZRA mode (Fig. 3). In the portable cell, the same behaviour of the PSDs can be observed in Fig. 11b, with a strong decrease of the PSD after the transition to passivation (curve *ii*). However, the PSD in the portable cell was much higher (two orders of magnitude at 0.1 Hz) than in the lab-liquid cell after the transition (curve *iii*) and this higher level at frequencies below 1 Hz can also be noted later (curves *iv* and *v*). The persistence of corrosion reactions indicated by the still high level of noise when the electrode potential went back to the OCP is probably related to the higher accessibility of atmospheric oxygen to the metal-electrolyte interface in the portable cell than in the lab-liquid and lab-gel cells.

The observation of the samples by optical microscopy after the experiments confirmed that the potential fluctuations at the beginning of the tests correspond to pitting attack in liquid electrolyte as well as in both gel cells (Fig. 12). The pits were quite similar in size and shape in liquid and gel electrolytes. In galvanostatic mode, it was then possible in gel electrolyte to obtain small metastable pits like those in liquid electrolyte, while the potentiostatic mode led to large stable pits.

4. Conclusions

Electrochemical noise measurements have been performed on stainless steel in liquid and gel NaCl aqueous solutions using different modes (ZRA, galvanostatic, potentiostatic). To the best of our knowledge, this is the first time that EN measurements carried out with a commercial potentiostat using all modes were validated with power spectral densities overlapping in common frequency ranges when the noise signals were stationary. It is shown that the EN technique can be used with gelled electrolytes to detect localized corrosion and study the passivity of stainless steels. It was also confirmed that the risk of crevice corrosion is reduced with the portable-gel cell in comparison with cells in which the surface of the WE is delimited by an epoxy coating.

Different EN results were obtained, depending on the electrochemical cell design and polarization control method. In ZRA mode, current transients generated by metastable pitting were less numerous and of a smaller amplitude in the agar gelled electrolyte, mainly because of mass transport limitation of the corrosion reactions. In potentiostatic mode at potential above 150 mV *vs.* SCE, the repassivation of the metastable pits was very sudden in both liquid and gel electrolytes, in contrast with the other modes. However, stable pits were also formed in gelled electrolyte, much faster in the lab-gel cell than in the portable cell, which was not observed in the liquid electrolyte of same chloride content. When the stainless steel electrode was galvanostatically polarized at a current density of 1.25 $\mu A/cm^2$, the amplitude of the voltage transients initially caused by pitting corrosion increased with time and the electrode ended up oscillating between active and passive states until repassivation occurred.

Acknowledgements: The authors are thankful to the University Carlos III of Madrid for the financial support through the mobility grant of Gleidys Monrrabal in Paris (2017).

Data availability

The raw/processed data required to reproduce these findings cannot be shared at this time due to technical or time limitations.

References

[1] T. Hagyard, M.J. Prior, Potential of aluminium in aqueous chloride solutions, part 2, Trans. Faraday Soc. 57 (1961) 2295–2298. http://doi.org/10.1039/TF9615702295.

[2] W.P. Iverson, Transient voltage changes produced in corroding metals and alloys, J. Electrochem. Soc. 115 (1968) 617–618. http://doi.org/10.1149/1.2411362.

[3] C. Gabrielli, F. Huet, M. Keddam, R. Oltra, A review of the probabilistic aspects of localized corrosion, Corrosion 46 (1990) 266–278. http://doi.org/10.5006/1.3585102.

[4] J.R. Kearns, J.R. Scully, P.R. Roberge, D.L. Reichert, J.L. Dawson (Eds.) EN Measurement for Corrosion Applications. STP 1277, American Society for Testing and Materials, West Conshohocken, 1996. http://doi.org/10.1520/STP1277-EB.

[5] R.E. Ricker, U. Bertocci, A review of EN and its application to the study of stress corrosion cracking, in: R.H. Jones, D.R. Baer (Eds.) New Techniques for Characterizing Corrosion and Stress Corrosion, Warrendale, TMS-Miner Metals and Materials Society, 1996, pp 235–245.

[6] R.A Cottis, S. Turgoose, Corrosion Testing Made Easy: Electrochemical Impedance and Noise, Houston: NACE, 1999.

[7] R.A. Cottis, Interpretation of electrochemical noise data, Corrosion 57 (2001) 265–284. http://doi.org/10.5006/1.3290350.

[8] F. Huet, Electrochemical noise technique, in: P. Marcus, F. Mansfeld, (Eds.), Analytical Methods in Corrosion Science and Enginering, Taylor & Francis, Boca Raton 2005, pp. 507–570.

[9] D.A. Eden, K. Hladky, D.G. John, J.L. Dawson. EN — simultaneous monitoring of potential and current noise signals from corroding electrodes. CORROSION'86, Houston, NACE, 1986, Paper 274, pp 1–9.

[10] F. Mansfeld, H. Xiao, Electrochemical noise analysis of iron exposed to NaCl solutions of different corrosivity, J. Electrochem. Soc. 140 (1993) 2205–2209. http://doi.org/10.1149/1.2220796.

[11] A. Aballe, A. Bautista, U. Bertocci, F. Huet, Measurement of the noise resistance for corrosion applications, Corrosion 57 (2001) 35–42. http://doi.org/10.5006/1.3290327.

[12] V. Di Noto, S. Lavina, G.A. Giffin, E. Negro, B. Scrosati, Polymer electrolytes: Present, past and future, Electrochim. Acta. 57 (2011) 4–13. http://doi.org/10.1016/j.electacta.2011.08.048.

[13] E. Cano, A. Crespo, D. Lafuente, B. Ramirez Barat, A novel gel polymer electrolyte cell for in-situ application of corrosion electrochemical techniques, Electrochem. Commun. 41 (2014) 16–19. http://doi.org/10.1016/j.elecom.2014.01.016.

[14] B. Ramírez Barat, E. Cano, The use of agar gelled electrolyte for in situ electrochemical measurements on metallic cultural heritage, Electrochim. Acta 182 (2015) 751–762. http://doi.org/10.1016/j.electacta.2015.09.116.

[15] E. Angelini, S. Grassini, M. Parvis, F. Zucchi, An in situ investigation of the corrosion behaviour of a weathering steel work of art, Surf. Interface Anal. 44 (2012) 942–946. http://doi.org/10.1002/sia.3842.

[16] G. Monrrabal, S. Guzmán, I.E. Hamilton, A. Bautista, F. Velasco, Design of gel electrolytes for electrochemical studies on metal surfaces with complex geometry, Electrochim. Acta 220 (2016) 20–28. http://doi.org/10.1016/j.electacta.2016.10.081.

[17] G. Monrrabal, B. Ramírez-Barat, A. Bautista, F. Velasco, E. Cano, Non-destructive electrochemical testing for stainless-steel components with complex geometry using innovative gel electrolytes, Metals 8 (2018) 500. http://doi.org/10.3390/met8070500.

[18] F. Huet, S. Ritter, Electrochemical noise measurements with dummy cells: Evaluation of a round-robin test series, Corrosion, in press, https://doi.org/10.5006/3007.

[19] S. Ritter, F. Huet, R. A. Cottis, Guideline for an assessment of electrochemical noise measurement devices, Mater. Corros. 63 (2012) 297–302. http://doi.org/10.1002/maco.201005839.

[20] U. Bertocci, F. Huet, Noise resistance applied to corrosion measurements: III. Influence of the instrumental noise on the measurements, J. Electrochem. Soc. 144 (1997) 2786–2793. http://doi.org/10.1149/1.1837896.

[21] P.C. Pistorius, G.T. Burstein, Metastable pitting corrosion of stainless steel and the transition to stability, Phil. Trans. R. Soc. Lond. A 341 (1992) 531–559. http://doi.org/10.1098/rsta.1992.0114.

[22] A.J. Betts, L.H. Boulton, Crevice corrosion: review of mechanisms, modelling, and mitigation, Brit. Corros. J. 28 (1993) 279–296. http://doi.org /10.1179/000705993799156299.

[23] R. Qvarfort, New electrochemical cell for pitting corrosion testing, Corros. Sci. 28 (1988) 135–140. http://doi.org/10.1016/0010-938X(88)90090-X.

[24] C. Gabrielli, F. Huet, M. Keddam, Investigation of electrochemical processes by an electrochemical noise analysis. Theoretical and experimental aspects in potentiostatic regime, Electrochim. Acta 31 (1986) 1025–1039. http://doi.org/10.1016/0013-4686(86)80018-4.

[25] F. Huet, K. Ngo, Electrochemical noise - Guidance for improving measurements and data analysis, CORROSION 2018, Houston, NACE, 2018, Paper 11042, pp 1–11.

LIST OF CAPTIONS

Table 1

Chemical composition (wt. %) of the stainless steel used in this study.

Table 2

Phenomena occurring on the SS electrodes under different anodic polarizations in the three electrochemical cells.

Fig.1. Electrochemical cell set-ups used for EN measurements (a) in ZRA mode and (b) in galvanostatic and potentiostatic modes in the lab-liquid and lab-gel cells; (c) in the portable gel cell.

Fig. 2. Time records of the current and voltage fluctuations sampled at 1 Hz in ZRA mode after 2h 20 min of electrode immersion in (a) the lab-liquid cell (curve sampled at 10 Hz in the insert), (b) the lab-gel cell.

Fig. 3. PSDs of the (a) voltage and (b) current noises shown in Figure 2 for both lab-liquid and lab-gel cells.

Fig. 4. Z_n values for the SS electrodes in liquid and gel electrolytes obtained from EN measurements carried out in ZRA mode and impedance moduli $|Z|$ of the electrodes measured by EIS at the OCP.

Fig. 5. Polarization curves of the SS electrodes in the three electrochemical cells (sweeping rate 1.2 mV/s).

Fig. 6. Differences in oxygen concentration close to the WE edge: (a) conventional electrode with surface area delimited by epoxy resin in liquid or gel electrolytes, (b) innovative portable cell with gel electrolyte.

Fig. 7. (a) Time record of the current fluctuations sampled at 100 Hz when the SS WE was polarized at 200 mV *vs*. SCE at time 0 in the lab-liquid cell; (b) PSDs of the current fluctuations

sampled successively (*i*: f_s = 100 Hz during 5 min, *ii*: f_s = 10 Hz during 9 min, *iii*: f_s = 1 Hz during 120 min, *iv*: f_s = 100 Hz during 5 min).

Fig. 8. Time records of the current fluctuations when the SS WE was polarized at 200 mV *vs.* SCE at time 0: (a) in the lab-gel cell (f_s = 100 Hz); (b) in the portable-gel cell (f_s = 1 Hz).

Fig. 9. Optical microscopy images showing the morphology and size of pits obtained after potentiostatic EN measurements carried out at 200 mV *vs.* SCE: (a) in the lab-liquid cell; (b) in the lab-gel cell.

Fig. 10. Time records of the potential fluctuations carried out successively at 100 Hz (*i*), 10 Hz (*ii*) and 1 Hz (*iii*) under galvanostatic control in the three cells. The full dots indicate the times at which the anodic current density of 1.25 µA cm^{-2} was applied.

Fig. 11. PSDs of the voltage fluctuations sampled successively (*i*: f_s = 100 Hz during 5 min, *ii*: f_s = 10 Hz during 9 min, *iii*: f_s = 1 Hz during 120 min, *iv*: f_s = 100 Hz during 5 min) when the SS WE was polarized at 1.25 µA cm^{-2} (a) in the lab-liquid cell, and (b) in the portable cell.

Fig. 12. Optical microscopy images showing the morphology and size of pits obtained after galvanostatic EN measurements carried out at a current density of 1.25 µA cm^{-2}: (a) in the lab-liquid cell; (b) in the portable-gel cell.

Table 1

Chemical composition (wt. %) of the stainless steel used in this study.

Element	Si	P	Ti	V	Cr	Mn	Ni	Cu	Nb	Mo	C	S	N	Fe
%	0.30	0.025	0.007	0.07	18.66	1.82	8.06	0.24	0.115	0.19	0.043	0.005	0.048	Bal.

Table 2

Phenomena occurring on the SS electrodes under different anodic polarizations in the three electrochemical cells.

Cell	Anodic polarization (mV *vs*. SCE)			
	150	200	300	350
Lab-liquid	Metastable pits	Metastable pits *(sometimes with crevice)*	Metastable pits *+ Crevice*	Metastable pits *+ Crevice*
Lab-gel	No pits	Metastable and stable pits *(sometimes with crevice)*	Metastable and stable pits *(sometimes with crevice)*	Metastable and stable pits *(sometimes with crevice)*
Portable-gel	No pits	Metastable and stable pits	Metastable and stable pits	Metastable and stable pits

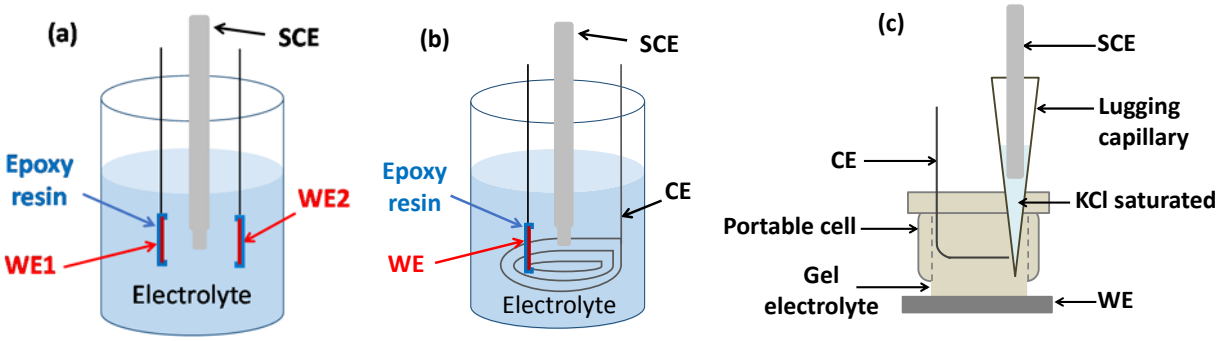

Fig.1. Electrochemical cell set-ups used for EN measurements (a) in ZRA mode and (b) in galvanostatic and potentiostatic modes in the lab-liquid and lab-gel cells; (c) in the portable gel cell.

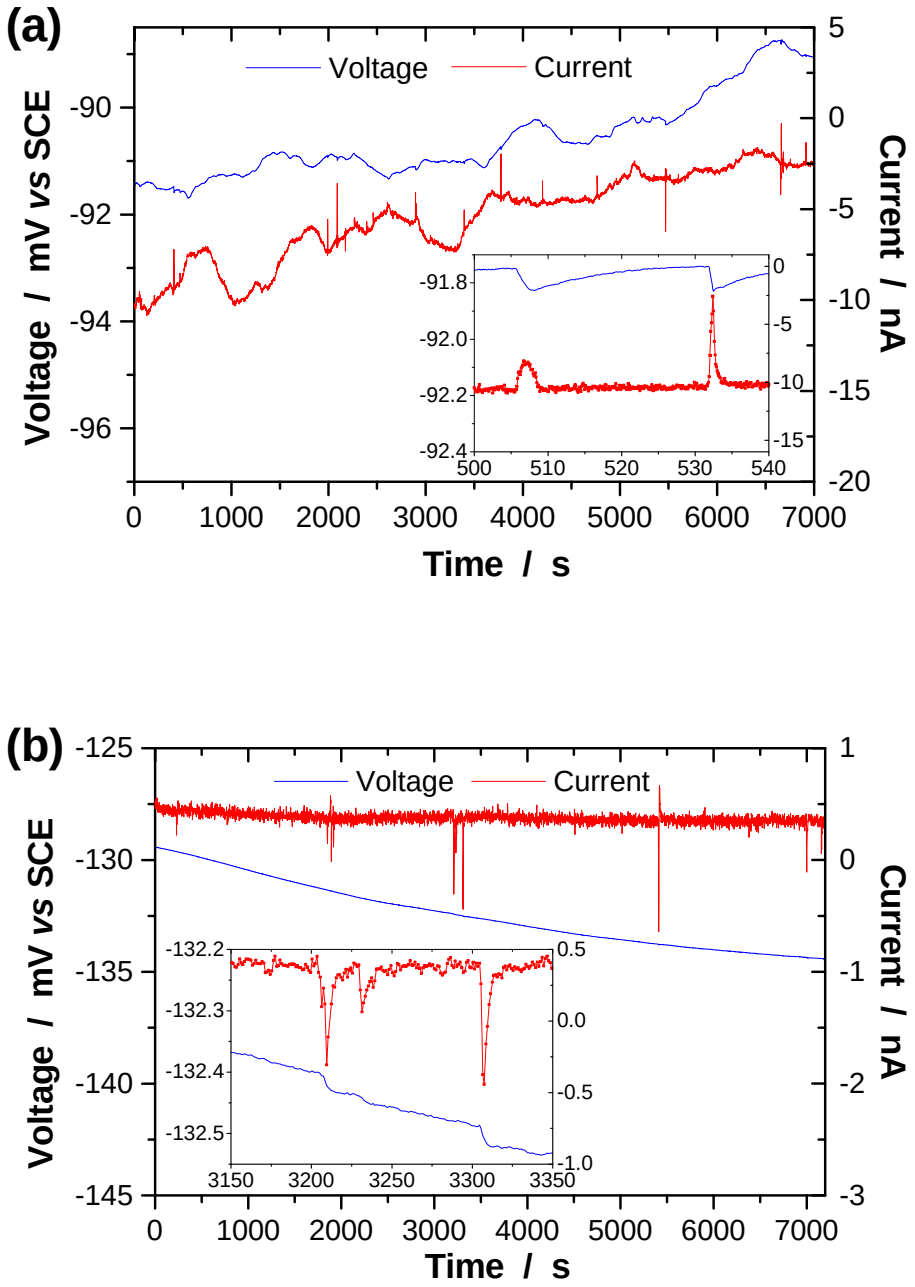

Fig. 2. Time records of the current and voltage fluctuations sampled at 1 Hz in ZRA mode after 2h 20 min of electrode immersion in (a) the lab-liquid cell (curve sampled at 10 Hz in the insert), (b) the lab-gel cell.

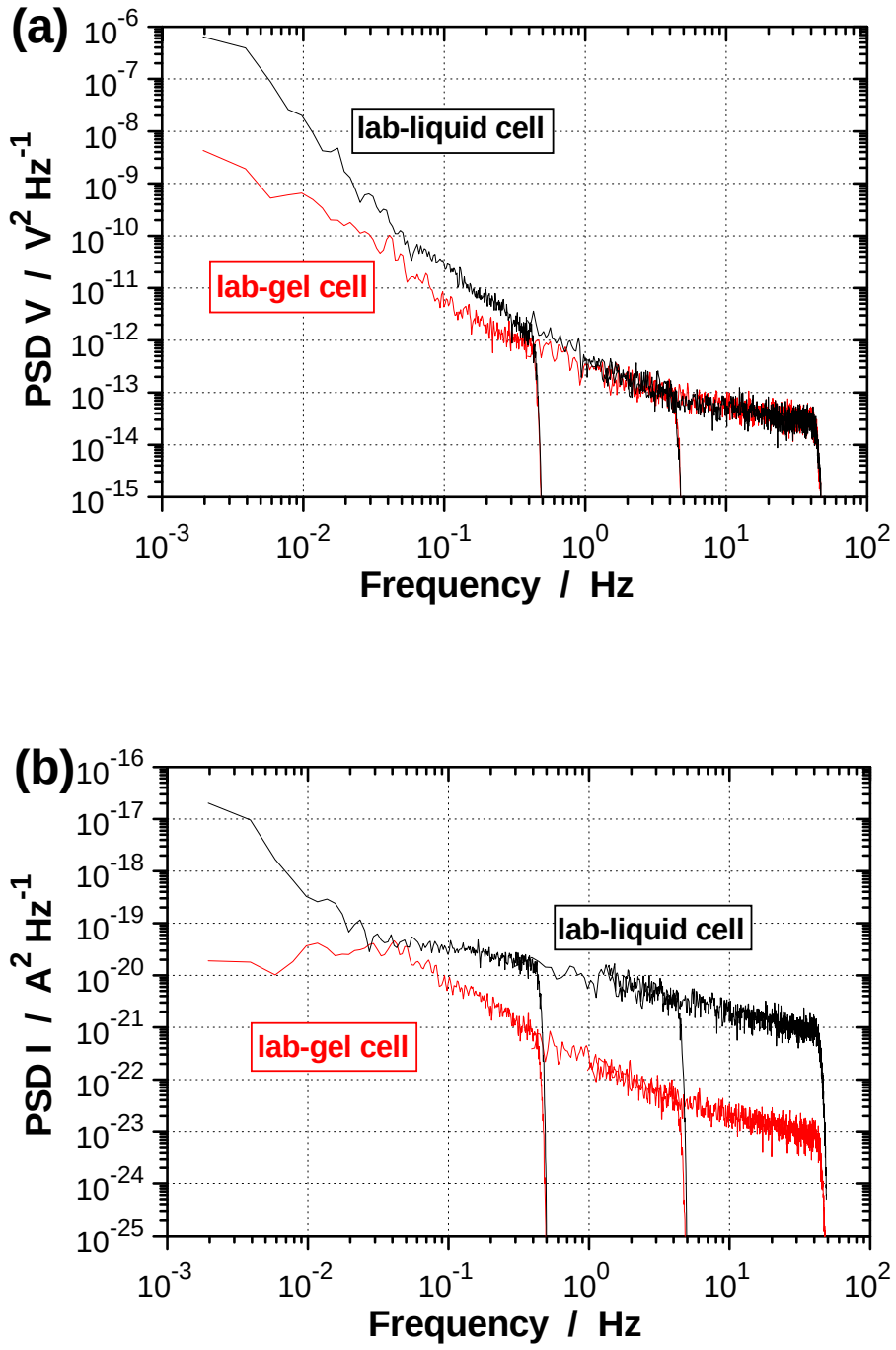

Fig. 3. PSDs of the (a) voltage and (b) current noises shown in Figure 2 for both lab-liquid and lab-gel cells.

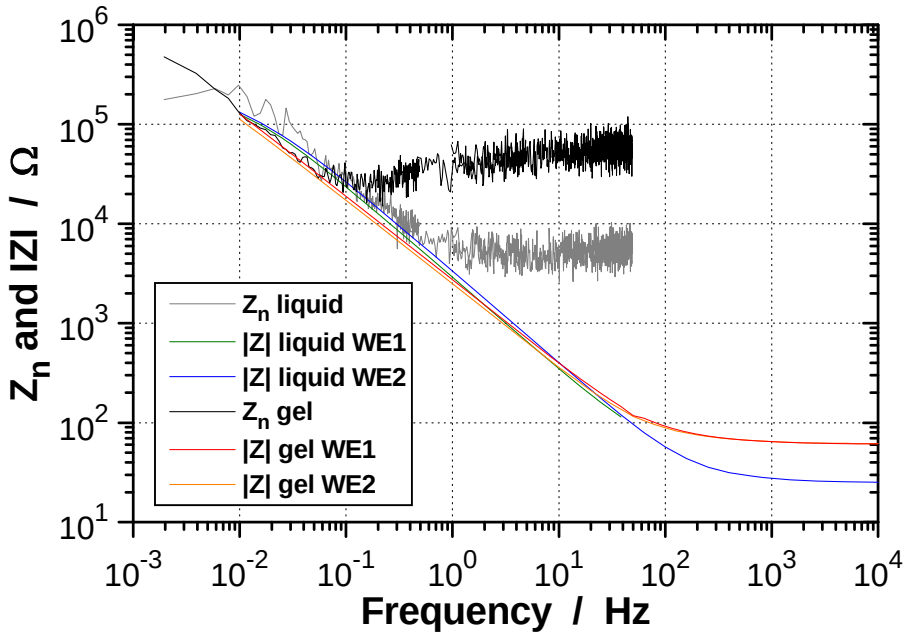

Fig. 4. Z_n values for the SS electrodes in liquid and gel electrolytes obtained from EN measurements carried out in ZRA mode and impedance moduli |*Z*| of the electrodes measured by EIS at the OCP.

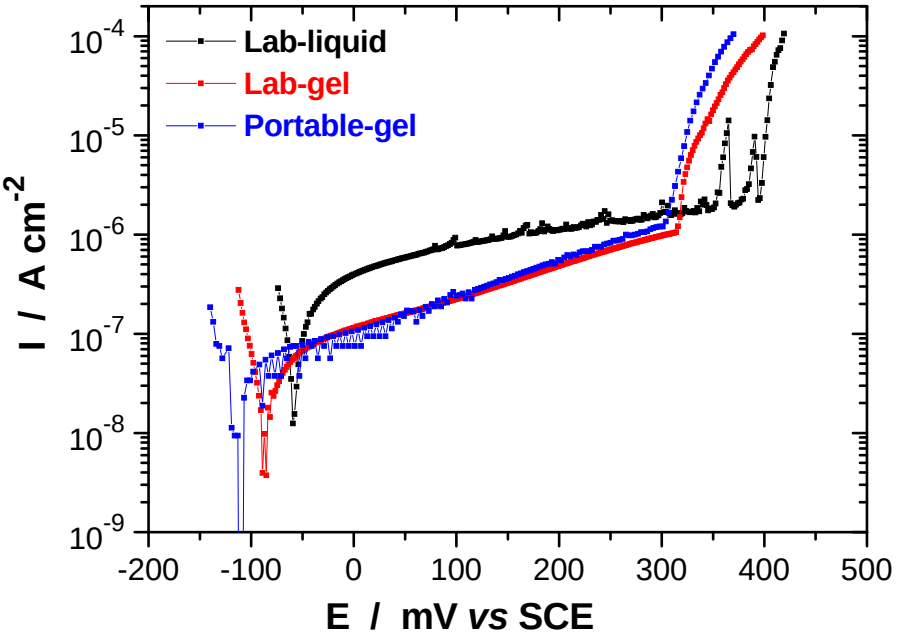

Fig. 5. Polarization curves of the SS electrodes in the three electrochemical cells (sweeping rate 1.2 mV/s).

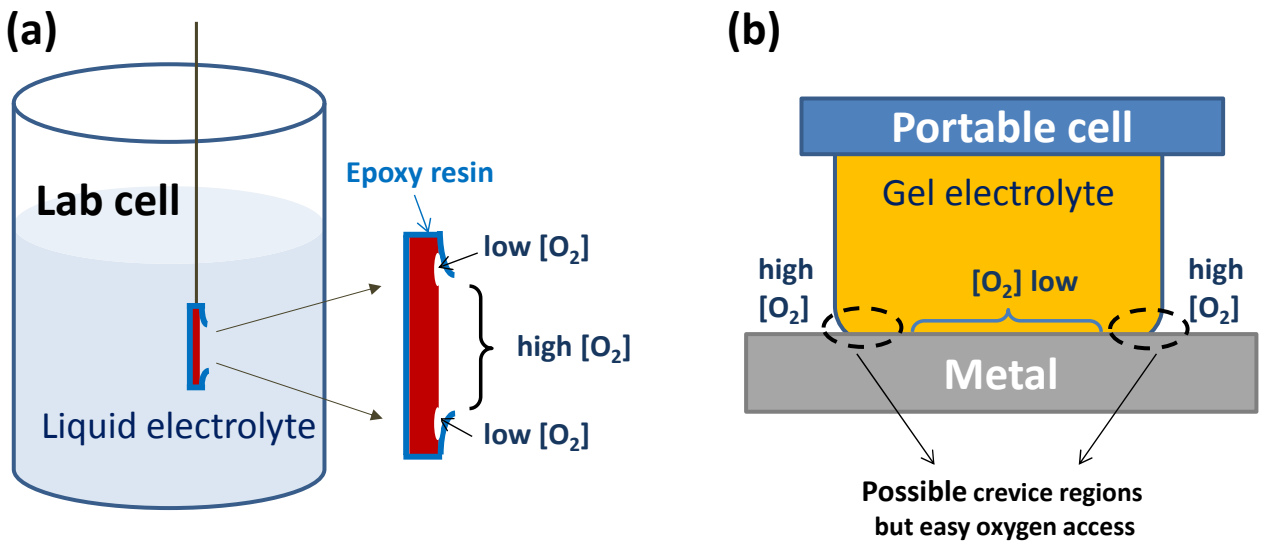

Fig. 6. Differences in oxygen concentration close to the WE edge: (a) conventional electrode with surface area delimited by epoxy resin in liquid or gel electrolytes, (b) innovative portable cell with gel electrolyte.

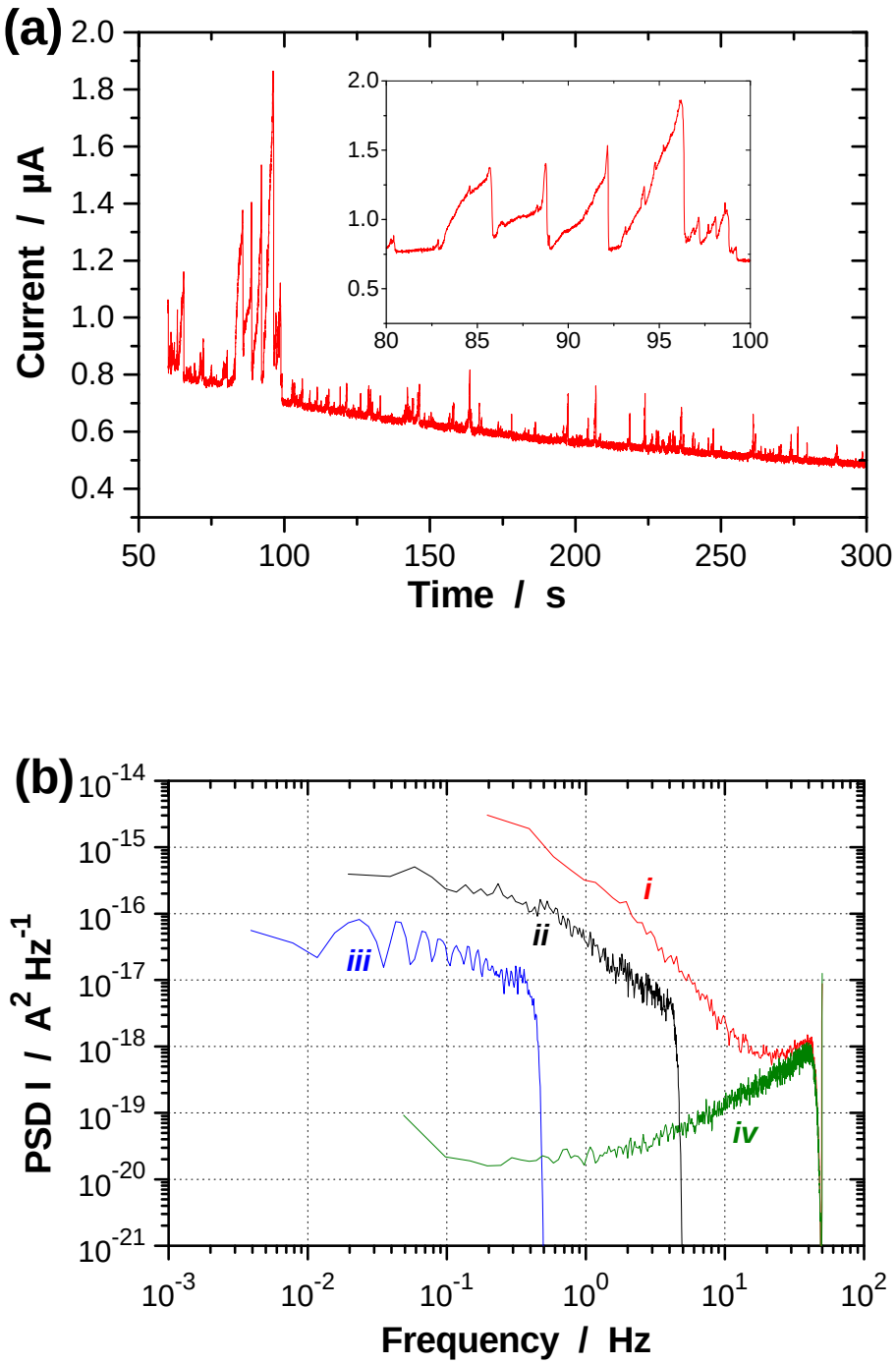

Fig. 7. (a) Time record of the current fluctuations sampled at 100 Hz when the SS WE was polarized at 200 mV *vs*. SCE at time 0 in the lab-liquid cell; (b) PSDs of the current fluctuations sampled successively (*i*: f_s = 100 Hz during 5 min, *ii*: f_s = 10 Hz during 9 min, *iii*: f_s = 1 Hz during 120 min, *iv*: f_s = 100 Hz during 5 min).

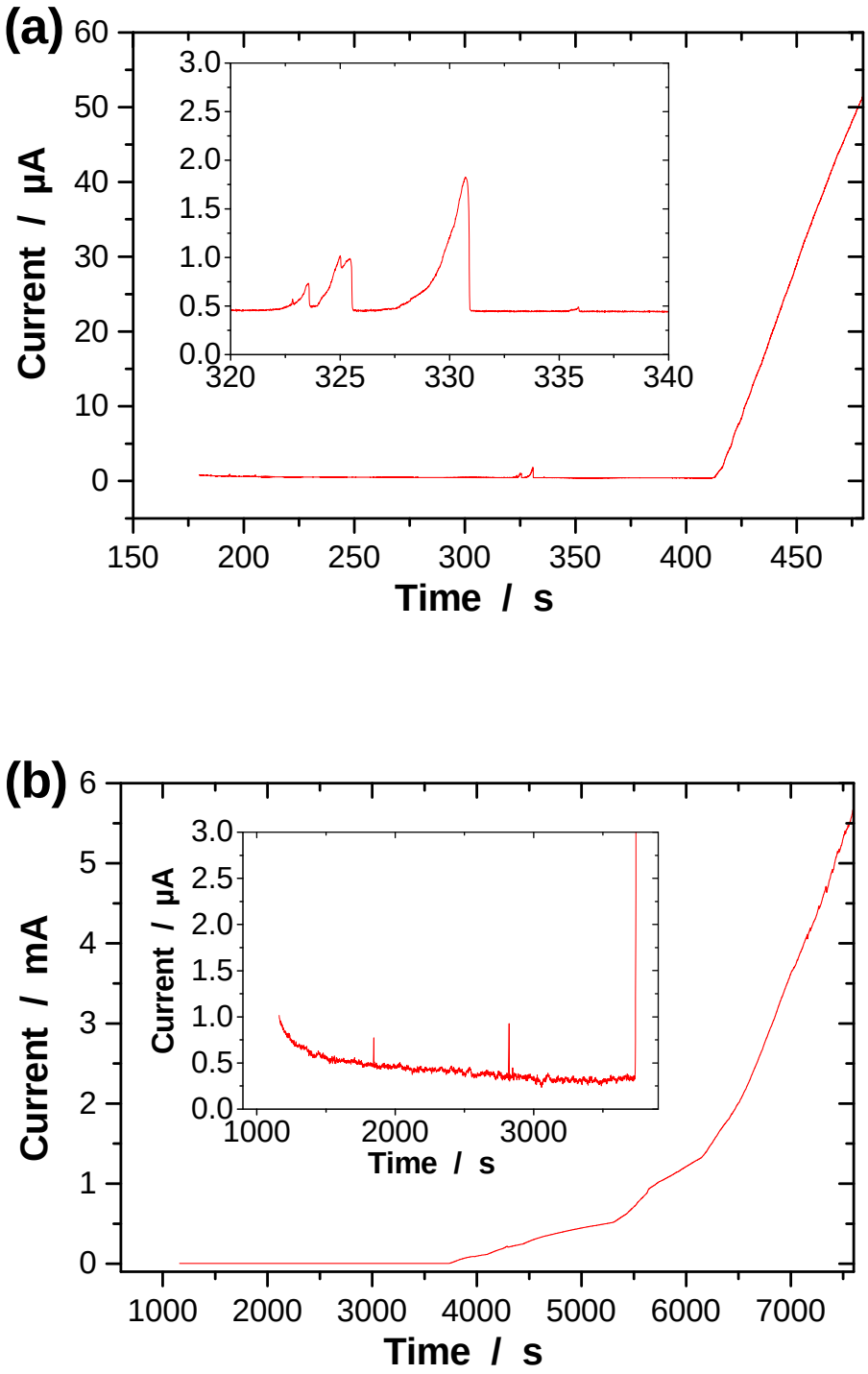

Fig. 8. Time records of the current fluctuations when the SS WE was polarized at 200 mV *vs*. SCE at time 0: (a) in the lab-gel cell (f_s = 100 Hz); (b) in the portable-gel cell (f_s = 1 Hz).

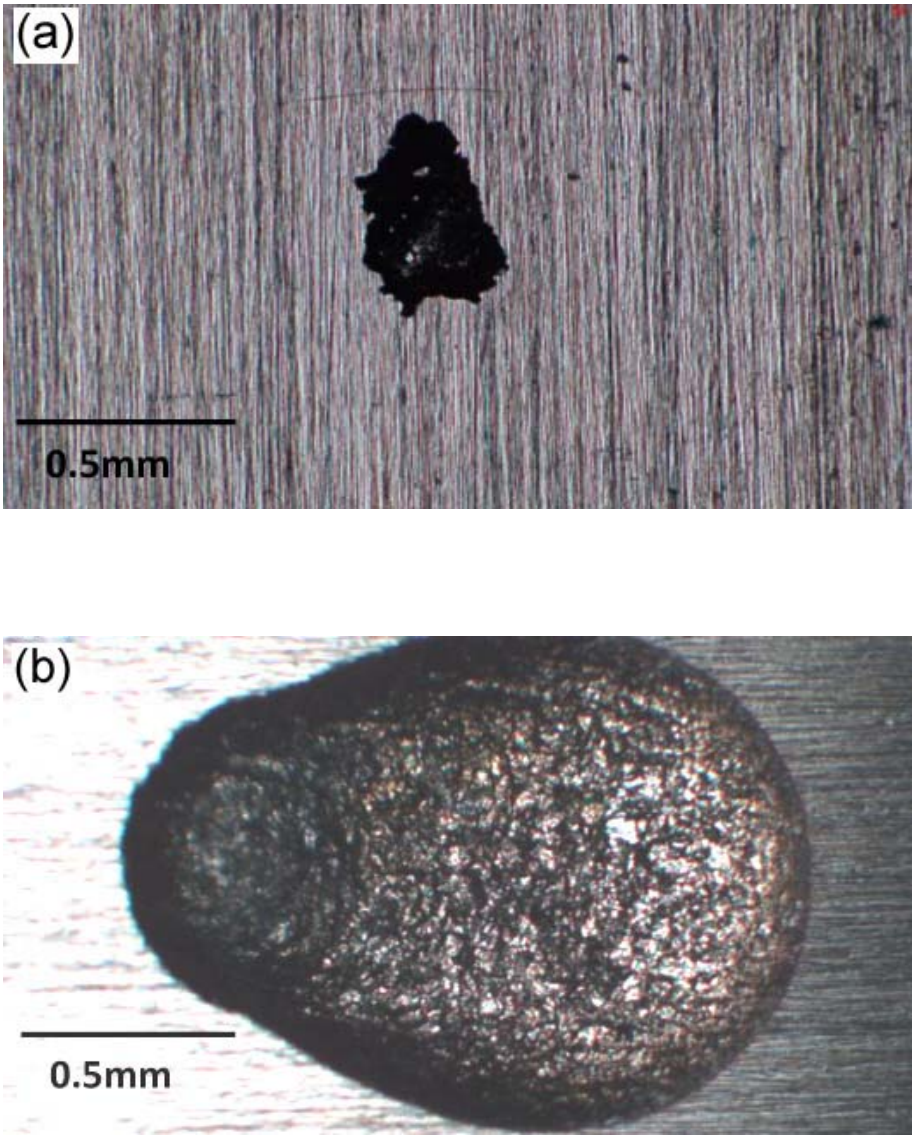

Fig. 9. Optical microscopy images showing the morphology and size of pits obtained after potentiostatic EN measurements carried out at 200 mV *vs.* SCE: (a) in the lab-liquid cell; (b) in the lab-gel cell.

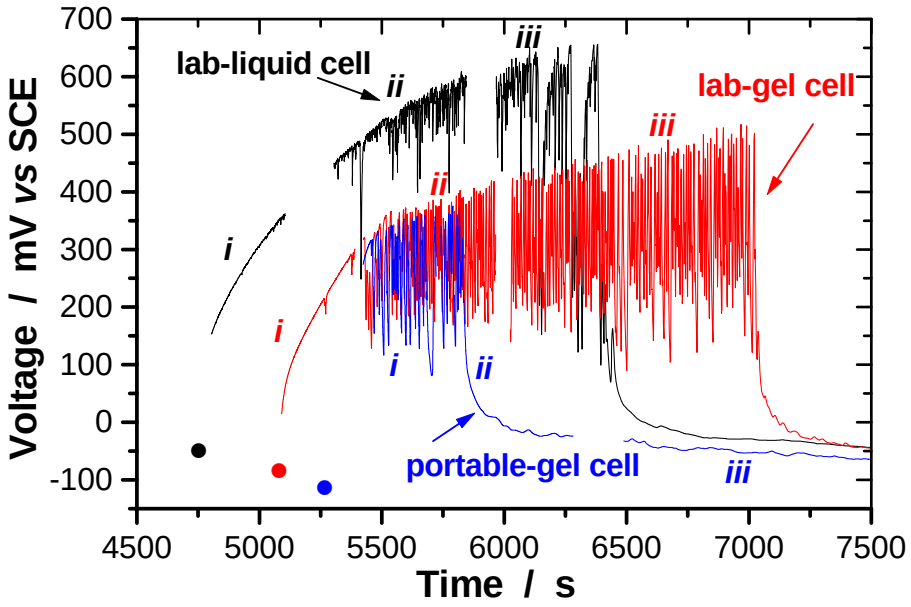

Fig. 10. Time records of the potential fluctuations carried out successively at 100 Hz (*i*), 10 Hz (*ii*) and 1 Hz (*iii*) under galvanostatic control in the three cells. The full dots indicate the times at which the anodic current density of 1.25 µA cm^{-2} was applied.

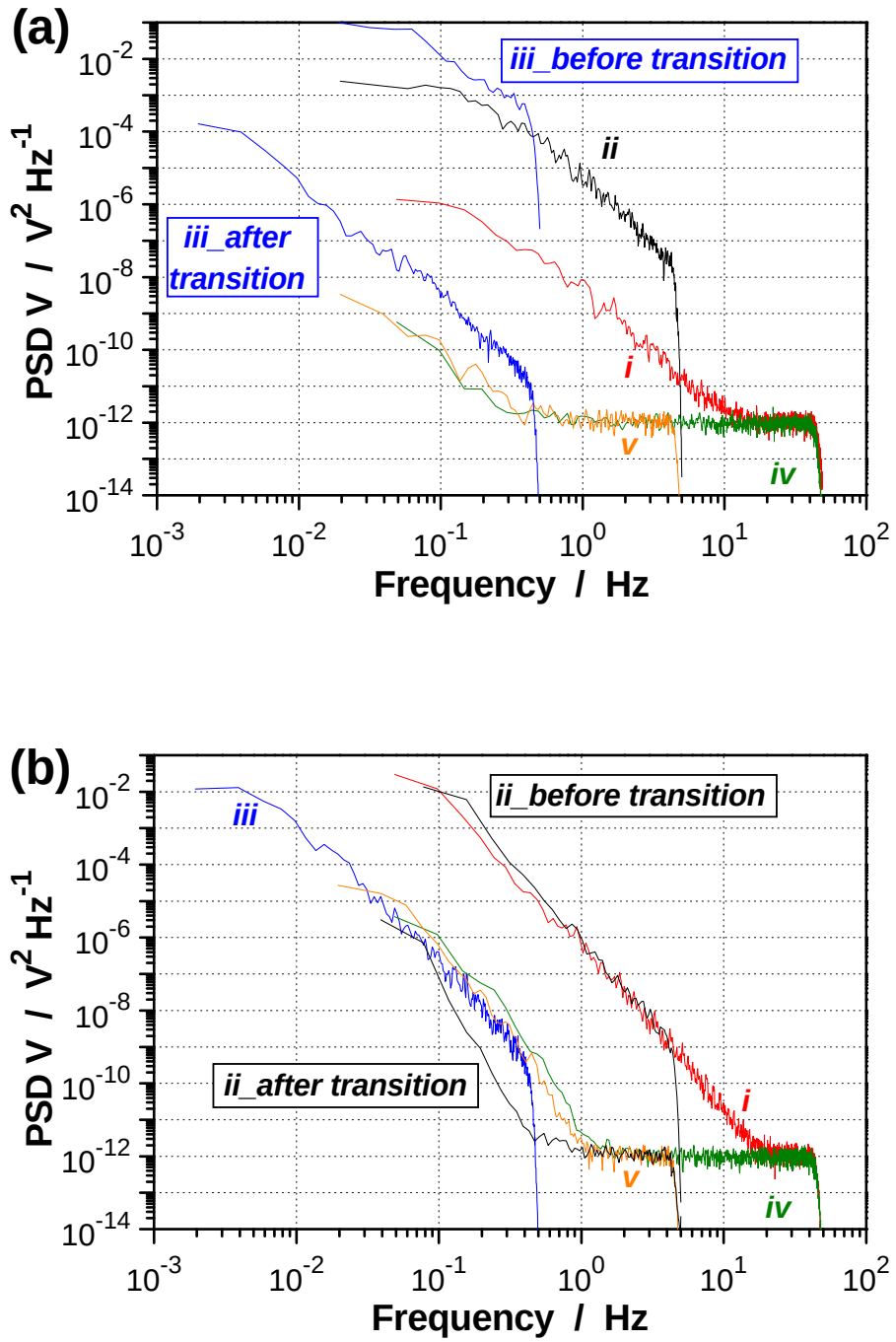

Fig. 11. PSDs of the voltage fluctuations sampled successively (*i*: f_s = 100 Hz during 5 min, *ii*: f_s = 10 Hz during 9 min, *iii*: f_s = 1 Hz during 120 min, *iv*: f_s = 100 Hz during 5 min) when the SS WE was polarized at 1.25 µA cm^{-2} (a) in the lab-liquid cell, and (b) in the portable cell.

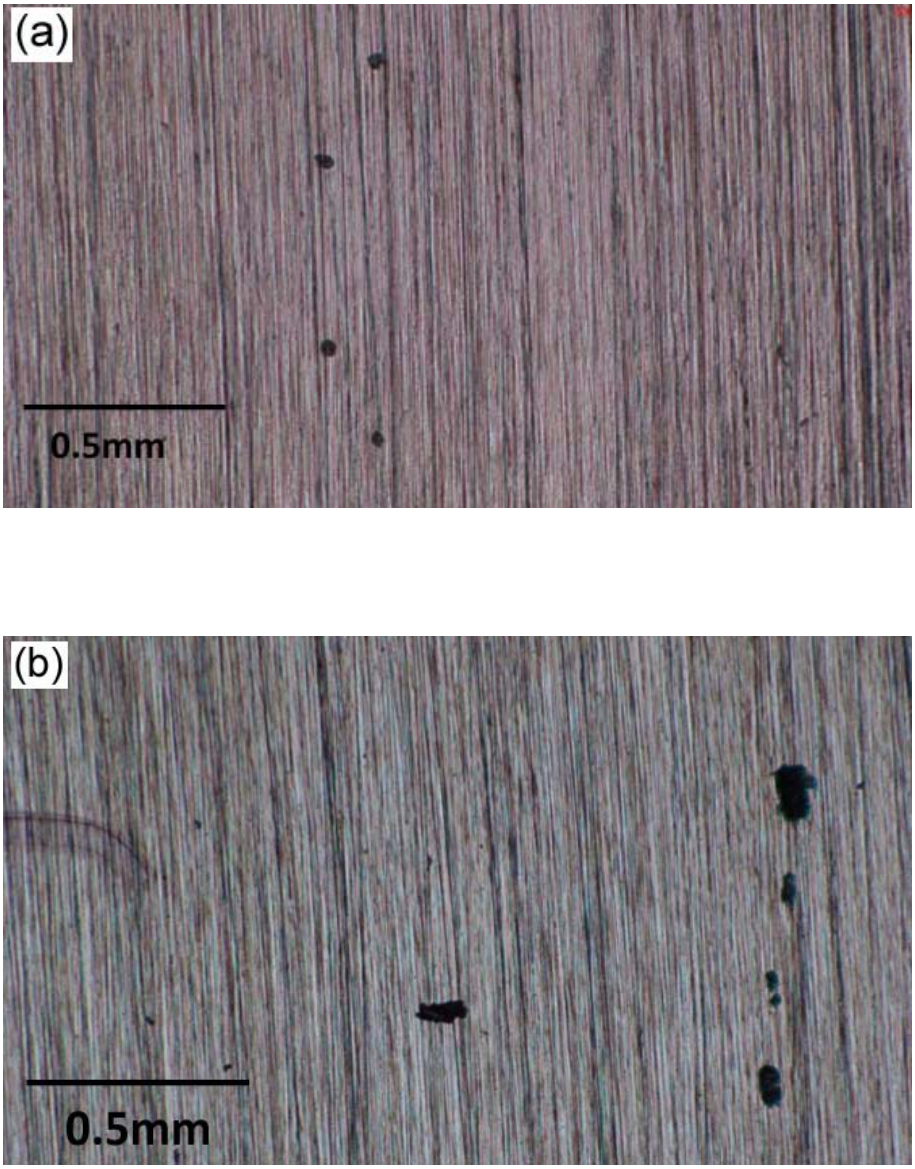

Fig. 12. Optical microscopy images showing the morphology and size of pits obtained after galvanostatic EN measurements carried out at a current density of 1.25 μA cm^{-2}: (a) in the lab-liquid cell; (b) in the portable-gel cell.